Experimental barrier distributions for the fusion of ^{12}C, ^{16}O, ^{28}Si, and ^{35}Cl with ^{92}Zr and coupled-channels analyses

J. O. Newton, C. R. Morton, M. Dasgupta, J. R. Leigh, J. C. Mein, D. J. Hinde, and H. Timmers
Department of Nuclear Physics, Research School of Physical Sciences and Engineering, Australian National University, Canberra ACT 0200, Australia

K. Hagino
Yukawa Institute for Theoretical Physics, Kyoto University, Kyoto 606-8502, Japan
(Received 1 June 2001; published 20 November 2001)

Precise excitation functions for the fusion of ^{12}C, ^{16}O, ^{28}Si, and ^{35}Cl on ^{92}Zr were measured for bombarding energies spanning the Coulomb barrier regions. Experimental fusion barrier distributions were derived from these data and compared with the results of realistic coupled-channels calculations, which included couplings to all orders and treated excitation energies correctly. To gain reasonable agreement for the heavier projectiles it was necessary to include double-phonon excitations of the first 2^+ and 3^- vibrational states in ^{92}Zr. The diffuseness parameter required to fit the high-energy cross sections increases with increasing charge of the projectile and, as found in earlier work, is higher than that required to fit elastic-scattering data. It is suggested that a potential which falls more rapidly at large distance than the Woods-Saxon form might help explain the anomaly.

DOI: 10.1103/PhysRevC.64.064608 PACS number(s): 25.70.Jj, 24.10.Eq, 21.60.Ev, 27.60.+j

I. INTRODUCTION

It used to be believed that the fusion of two nuclei could be described completely by the quantum mechanical penetration of a simple one-dimensional potential barrier. This treatment is indeed appropriate for the fusion of light nuclei with the charge product Z_1Z_2 for the projectile and target less than about 200. However for systems with larger charge products this treatment is not adequate. Simple theoretical prescriptions were developed which implicitly [1] or directly [2] introduced a distribution of barrier heights. Stokstad *et al.* [3] were the first to show experimentally that subbarrier fusion cross sections $\sigma_{\rm fus}$, much larger than expected on the basis of the simple one-dimensional picture, could be related to specific nuclear structure effects. It is now realized [4] that such enhancement of subbarrier fusion cross sections arises from coupling between the elastic channel and intrinsic degrees of freedom of the target and projectile. Important degrees of freedom are those corresponding to nuclear deformation and vibration and particle transfer. When these couplings are taken into account in the eigenchannel model [5,6], the simple one-dimensional barrier can be thought of as splitting into a distribution of discrete barriers. These barriers are distributed in energy about the average barrier, with a weight which represents the probability of encountering that barrier. This splitting drastically modifies the probability for fusion and leads to an enhancement of the subbarrier fusion cross sections over those predicted by a single-barrier model.

It was demonstrated by Rowley *et al.* [7] that a representation of the distribution of barriers could be obtained by taking the second derivative of the product $E_{\rm c.m.}\sigma_{\rm fus}$ as a function of center-of-mass energy $E_{\rm c.m.}$. The quantity $d^2(E_{\rm c.m.}\sigma_{\rm fus})/dE^2_{\rm c.m.}$ will be referred to as the barrier distribution. Its measurement requires very precise determination of fusion cross sections at closely spaced and precisely defined energy intervals. Such measurements were pioneered by Leigh *et al.* [8–12] and, since then, have been carried out by a number of groups [4]. The measured barrier distributions are sensitive to the structure of target and projectile nuclei. They also have an advantage in that it is much easier to see the detailed effects of the couplings in the barrier distribution than in an exponentially changing fusion excitation function though, of course, the same information is carried in both.

To interpret the meaning of an experimental barrier distribution requires comparison with a barrier distribution derived from a coupled-channels (CC) calculation. Until recently such comparisons were made with simplified codes such as CCFUS [13] and its derivatives such as CCMOD [14]. However, the precision of the data showed that the approximations inherent in these codes were not adequate, and this has led to the use of more exact CC codes such as CCFULL [15]. This treats the excitation energies of the coupled states correctly, and avoids the use of the linear coupling approximation, whereby only the first term in the nuclear coupling potential expanded in terms of the deformation parameter is included. It has been shown [16–18] that it is necessary to include higher-order terms in this expansion when the coupling, which is approximately proportional to Z_1Z_2, is large.

Although our understanding of barrier distributions has increased greatly over recent years, there is still much that is not well understood. Systematic studies are usually more informative than those for individual cases, since it is likely that more can be learned by making comparisons between reactions that involve a common projectile or target. Thus the measurements described in this work were undertaken in order to see whether it would be possible to derive reasonably consistent fits to the barrier distributions for a sequence of progressively heavier projectiles bombarding the same target nucleus. The target nucleus chosen was ^{92}Zr and the projectile nuclei were ^{12}C, ^{16}O, ^{28}Si, and ^{35}Cl. The experi-

 ©2001 The American Physical Society

TABLE I. The beam-energy ranges (inclusive) and energy steps for the four fusion reactions initiated by the given projectiles on ^{92}Zr.

Projectile	Energy range	Energy step (MeV)
^{12}C	31.0–44.0	1.0
	46.0–50.0	2.0
^{16}O	44.0–50.0	0.5
	51.0–56.0	1.0
	58.0–80.0	2.0
^{28}Si	86.0–107.0	1.0
	115.0	
^{35}Cl	107.0–121.0	1.0
	123.0–127.0	2.0
	131.0–135.0	4.0

mental barrier distributions for the different systems were compared with calculations made with the realistic CC code CCFULL.

A coupled-channels description of fusion requires a number of inputs. These include the real nucleus-nucleus potential parameters and the coupling strengths and excitation energies of the important excited states. There is considerable uncertainty regarding the potential parameters. A conventional Woods-Saxon (WS) potential shape has usually been used, as in this work. However, there is no good reason why this should be the correct shape for heavy-ion interactions [19]. More reasonable shapes might be those of the proximity potential [20] or the folding potential [21], the latter being better approximated by a WS-squared potential than by the WS itself. However, it is still not clear whether these give a good representation of the potential between two heavy ions. Use of the WS potential may be responsible for the known discrepancy [12] between the much larger diffuseness parameters determined from fusion cross sections above the barrier region and those determined from elastic scattering, which probes larger separation distances than does fusion. It is also possible that this discrepancy might arise from an energy dependence of the ''bare'' potential, from neglect of other couplings [4], or angular momentum effects. Later in this work, the possibility that the discrepancy can be explained by potentials, which decrease more rapidly with separation distance than the WS, is explored.

II. EXPERIMENTAL PROCEDURE

The heavy ions, accelerated by the ANU 14UD Pelletron accelerator, were pulsed to provide ≈ 1 ns wide beam bursts every 530 ns. The beam energy ranges and energy steps used are given in Table I. The absolute beam energies were defined with an accuracy of $\pm 0.06\%$ and the relative beam energies to better than a few keV [12]. The zirconium targets were made by sputtering from a pellet of ZrO_2, isotopically enriched to 99.7% in ^{92}Zr, using an argon saddle-field ion source. The ^{92}Zr targets were $\approx 40\ \mu g\,cm^{-2}$ in thickness and deposited on carbon backings of $\approx 20\ \mu g\,cm^{-2}$.

The products from these reactions passed through a 1.5 mm diameter aperture, located 200 mm from the zirconium target, into a compact velocity filter [12,22]. This enabled separation of the evaporation residues (ERs) from the intense elastically scattered beam particles, which were subsequently prevented from entering a detector positioned downstream by a movable tantalum finger. The ERs were detected first in a position-sensitive multiwire proportional counter (MWPC), located behind the velocity filter and 600 mm from the target, and then in a thicker gas detector located behind the MWPC. The rear detector gave better energy and timing definition than did the MWPC. The ERs were identified by position, energy, and time of flight with respect to the pulsed beam. For larger angles, where elastic scattering was less intense and the ER yields small, the ERs were detected in a Si surface-barrier detector (SBD), which had approximately ten times the solid angle of the velocity filter, positioned at a precisely determined angle (typically $-20°$) relative to it. Here they were identified by total energy and time of flight. For the excitation functions, measurements were taken with the velocity filter at $\pm 2°$ to the beam direction. For angular distributions the velocity filter was typically moved in an angular range extending from $-5°$ to $+12°$, corresponding to an angular coverage of $2°$ to $25°$.

The ER yields were normalized by monitoring elastically scattered beam particles in two Si SBDs located at $30°$ symmetrically about the beam direction. The elastic scattering was assumed to be pure Rutherford to derive the absolute fusion cross sections. A small increase of $3.5 \pm 1.0\%$ in the cross section at the highest energy for the ^{12}C induced reaction was necessary as a consequence of diffraction effects. This was estimated from an optical-model calculation, using potential parameters derived from the $^{16}O + ^{90}Zr$ elastic scattering [23]. Measurements for the ^{16}O induced reaction were taken at energies much higher above the average barrier than for the other cases, and diffraction effects became significant at $30°$. For this reason the measurements for $E_{lab} \geqslant 48$ MeV were made with the monitors at $\pm 10°$. The monitor detectors were also used to measure and correct for slight changes in the angle of entry of the beam into the scattering chamber, and to calibrate the angle of the ER detector.

A. ER angular distributions

Full angular distributions were measured at a number of energies within the excitation functions for each reaction. The procedure for extracting the total fusion cross sections from the full angular distributions and the differential cross sections at $2°$, as well as a more detailed discussion of the experimental method, are outlined in Ref. [12]. One minor difference for these rather light systems was that the angular distributions were not so well fitted by two Gaussian functions, as previously used [12] for $^{16}O + ^{144,148,154}Sm$ and ^{186}W. A much better fit was achieved if the wider Gaussian, which is mainly a consequence of α emission, was replaced by a flat region, from $0°$ up to a certain angle, followed by a half Gaussian function. An example of such a fit to the data is shown in Fig. 1(a). That such a distribution should be a better fit was confirmed by calculations with the statistical model code PACE2 [24]. An example of such a fit to simu-

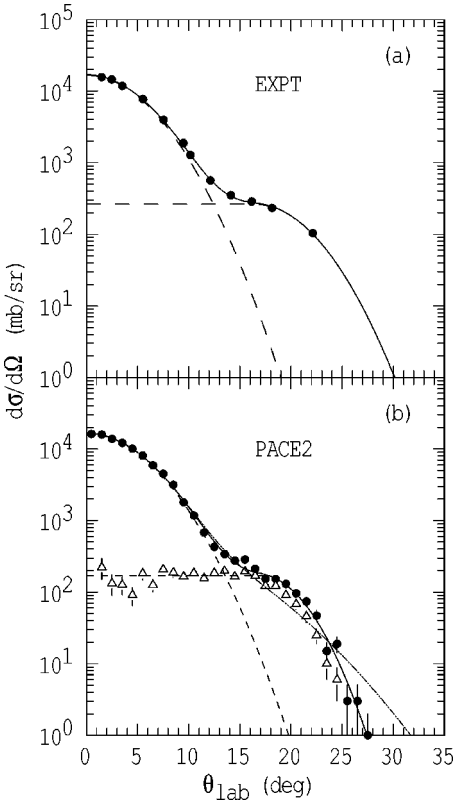

FIG. 1. ER angular distributions for $^{12}C+^{92}Zr$ at $E_{c.m.}=44.15$ MeV. (a) Experimental points fitted with the single Gaussian plus flat region and half Gaussian (full line) components are shown by the dashed lines. (b) Calculated with the PACE2 code (black points) and for the $\alpha 2n$ evaporation channel only (open triangles), fitted with two Gaussians (dash-dot-dotted curve) and with the single narrow Gaussian plus a flat region followed by a half Gaussian (solid line). The latter gives the better description of the angular distribution and its individual components are shown by the dashed lines.

lated data from PACE2 is shown in Fig. 1(b), where it is also compared with a two Gaussian fit. Use of the improved fit resulted in about a 1.5% reduction in deduced total cross section over that with the two Gaussian fit. However, the effect on the barrier distributions was negligible.

B. Extraction of the experimental barrier distribution

The barrier distribution was extracted from the experimental data according to a point-difference formula [12]. For the simple case of equal energy steps $\Delta E_{c.m.}$, the second derivative of $E_{c.m.}\sigma_{fus}$ at the c.m. energy E_n can be determined from

$$\frac{d^2(E_{c.m.}\sigma_{fus})}{dE^2}\approx\frac{(E\sigma_{fus})_{n+1}-2(E\sigma_{fus})_n+(E\sigma_{fus})_{n-1}}{(\Delta E_{c.m.})^2}. \quad (1)$$

For the single-barrier case, $d^2(E_{c.m.}\sigma_{fus})/dE^2_{c.m.}$ is related to the barrier distribution by a factor πR_B^2, where R_B is the radial separation of the two nuclei at the position of the average fusion barrier. The uncertainty in the second derivative δ_c is given by

$$\delta_c\approx\frac{E_n}{(\Delta E_{c.m.})^2}\sqrt{(\delta\sigma_{n+1})^2+4(\delta\sigma_n)^2+(\delta\sigma_{n-1})^2}, \quad (2)$$

where $\delta\sigma_i$ are the errors in the fusion cross sections. Hence the error on $d^2(E_{c.m.}\sigma_{fus})/dE^2_{c.m.}$ is proportional to the absolute errors in the fusion cross sections, and inversely proportional to the square of $\Delta E_{c.m.}$. At higher energies, where cross sections are large, practical considerations limit $\delta\sigma/\sigma$ to a constant value. Hence $\delta\sigma_i$ becomes proportional to σ_i and thus δ_c becomes proportional to σ, which increases with energy. The errors can be significantly reduced by increasing $\Delta E_{c.m.}$, but this is at the expense of smoothing the barrier distribution. Since the barriers themselves are smoothed by the effects of quantum mechanical tunneling, giving full widths at half maximum typically of 2–3 MeV, any additional smoothing caused by the step length is not a problem provided that $\Delta E_{c.m.}$ does not greatly exceed 2 MeV. The same procedure was used in deriving barrier distributions from theoretical calculations, so that a consistent comparison could be made between experiment and theory.

III. EXPERIMENTAL RESULTS AND ANALYSIS

The measured fusion cross sections for the four reactions are given in Table II. The errors shown for the cross sections are due to statistical uncertainties only. For these light systems, fission has negligible probability and hence the cross section for fusion is expected to be equal to that for the ERs. The fusion excitation functions and corresponding deduced barrier distributions for the four reactions are shown in Figs. 2–5. Preliminary information on the ^{28}Si induced reaction was given in Ref. [25]. The data are compared with the results of calculations with the simplified coupled-channels code CCMOD. The high-energy cross sections well above the average barrier should be relatively insensitive to the couplings. Hence, these were fitted using the Wong prescription for a single barrier [26], including the l dependence of the barrier position and ignoring deformation effects [27], to obtain the potential parameters required for CCMOD.

The nuclear potential was taken to be Woods-Saxon in form with

$$V_n(r)=-V_0/\{1+\exp[(r-r_0A_P^{1/3}-r_0A_T^{1/3})/a]\}, \quad (3)$$

where V_0 is the depth, r_0 is the radius parameter, and a is the diffuseness of the nuclear potential. The potential parameters obtained from the single-barrier fit to the high-energy data after fixing r_0 to 0.80 fm are given in Table III. The fusion cross sections and fusion barrier distributions from the single-barrier fit are shown by the dashed lines in Figs. 2–5.

IV. SIMPLIFIED CC CALCULATIONS

With the above potential parameters, an initial set of calculations was performed with the simplified coupled-

TABLE II. Fusion cross sections σ_{fus}, and their statistical errors $\delta\sigma$ at energies $E_{c.m.}$ for the indicated reactions. Energies where full angular distributions were measured are marked with an asterisk.

$E_{c.m.}$ (MeV)	σ_{fus} (mb)	$\delta\sigma$ (mb)	$E_{c.m.}$ (MeV)	σ_{fus} (mb)	$\delta\sigma$ (mb)
	$^{12}C + {}^{92}Zr$		64.64	1022	7
			66.34	1071	7
28.20	0.19	0.1	*68.05	1110	8
29.09	1.45	0.2	69.76	1159	8
29.98	2.91	0.2			
30.86	13.2	0.5		$^{28}Si + {}^{92}Zr$	
31.75	38.6	1.1			
*32.63	83.6	1.2	65.40	0.96	0.2
33.52	136	3	66.16	1.73	0.2
34.40	197	2	66.93	4.49	0.3
35.30	253	3	67.70	7.21	0.5
36.18	308	3	68.46	14.0	0.4
37.07	366	3	*69.23	23.6	0.6
*37.95	421	3	70.00	38.8	0.6
38.83	476	4	70.76	54.2	1.5
40.60	570	5	71.58	77.8	0.9
42.38	664	5	*72.30	94.9	1.3
*44.15	731	9	73.19	125	1
			73.83	141	1
	$^{16}O + {}^{92}Zr$		74.60	170	2
			75.36	197	2
37.35	0.23	0.07	*76.13	216	2
37.77	0.62	0.09	76.90	252	2
38.20	0.79	0.1	78.43	302	2
38.62	2.22	0.1	79.20	335	3
39.05	2.41	0.2	*79.96	365	3
39.47	4.62	0.3	80.73	383	3
39.90	8.7	0.4	81.50	404	3
40.33	15.2	0.5	*88.17	603	6
40.75	23.1	0.5			
41.18	33.8	0.6		$^{35}Cl + {}^{92}Zr$	
*41.61	49.2	0.5			
42.03	65.7	0.7	77.12	0.21	0.04
42.46	86.2	0.9	77.75	0.66	0.1
42.89	105	1	78.58	1.68	0.1
43.31	128	1	79.18	3.15	0.2
43.74	151	1	80.03	5.97	0.3
44.17	174	2	80.61	10.9	0.3
45.02	223	2	81.47	17.7	0.4
45.87	270	2	*82.06	26.6	0.3
46.30	299	2	82.92	42.6	0.6
*46.73	325	2	83.52	55.4	0.5
47.15	347	3	84.37	76.4	0.9
47.50	367	3	85.01	94.7	0.7
49.20	459	3	85.83	118	1
*50.99	543	3	86.41	135	1
52.70	626	5	87.41	165	1
54.40	687	5	88.73	207	1
56.11	754	6	90.18	254	2
57.81	813	6	*91.49	298	2
*59.52	867	6	94.40	376	2
61.23	912	7	97.30	459	3
62.93	971	7			

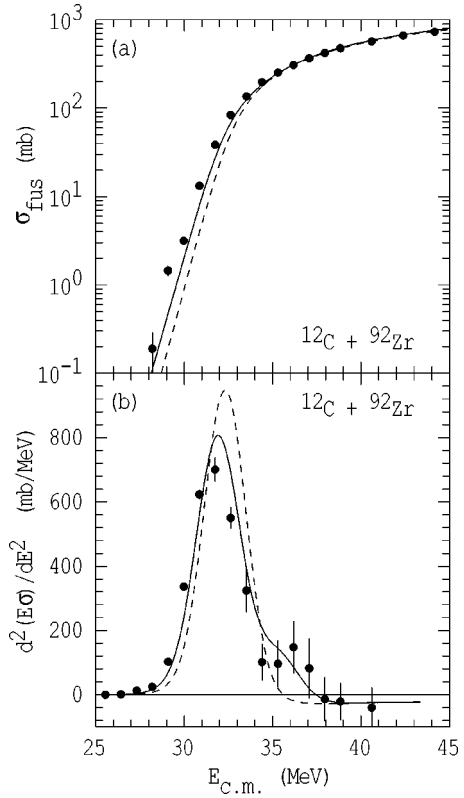

FIG. 2. The experimental (a) fusion cross sections and (b) barrier distribution for $^{12}C+^{92}Zr$, the latter evaluated with an energy step $\Delta E_{c.m.}=1.77$ MeV. Calculations with the simplified coupled-channels code CCMOD are shown for the uncoupled case (dashed lines) and with coupling to the ^{92}Zr states only (solid lines).

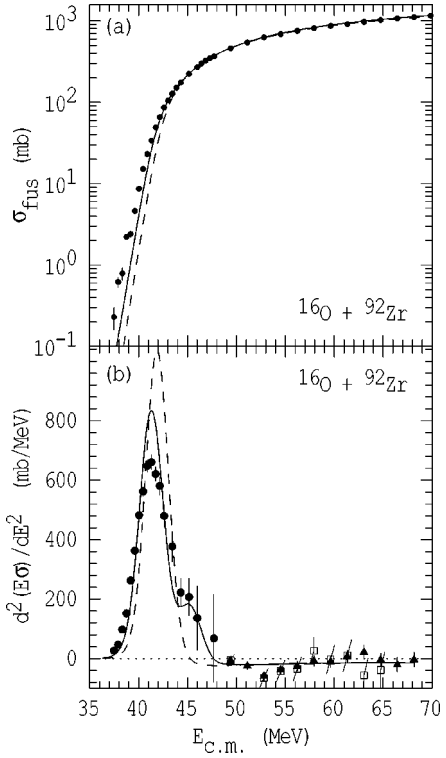

FIG. 3. The experimental (a) fusion cross sections and (b) barrier distribution for $^{16}O+^{92}Zr$, the latter evaluated with $\Delta E_{c.m.}=1.70$ MeV. At the higher energies, the energy step is 5.11 MeV for two separate measurements [triangular (repeated) and square data points]. The dashed line is a single-barrier calculation and the solid line is a CCMOD calculation with the first two excited states in ^{92}Zr.

channels code CCMOD. The lowest collective states of ^{92}Zr, the 2_1^+ and 3_1^- states, have excitation energies $\epsilon_2=0.934$ MeV [28] and $\epsilon_3=2.340$ MeV [29]. They are expected to be vibrational phonon, rather than rotational states. The deformation parameters associated with the multipolarity of the transition λ were obtained from the measured electromagnetic transition probabilities [28,29] using

$$\beta_\lambda=\frac{4\pi}{3ZR^\lambda}\left[\frac{B(E\lambda)\uparrow}{e^2}\right]^{1/2}, \tag{4}$$

where R is the radius of the nucleus which is excited, and is given by $R=r_cA^{1/3}$, with $r_c=1.06$ fm, as in previous analyses [12]. The resulting deformation parameters are $\beta_2=0.13$ and $\beta_3=0.25$.

The reaction $^{12}C+^{92}Zr$ has a low value of 240 for Z_1Z_2 and hence one might expect that the effect of couplings would be small and the effects of multiple excitations negligible. This is well borne out by the CCMOD calculation shown by the solid line in Fig. 2. Both the fusion excitation function and barrier distribution agree reasonably well with the experimental data and the difference between the uncoupled (dashed line) and coupled cases (solid line), though significant, is small.

The barrier distributions from the CCMOD calculations, where only the first 2^+ and 3^- states in ^{92}Zr were included, are given by the solid lines in Figs. 3, 4, and 5 for the ^{16}O, ^{28}Si, and ^{35}Cl reactions, respectively. The results from the simplified CC calculations provide a reasonable description of the barrier distributions for the ^{12}C and ^{16}O induced reactions, but as Z_1Z_2 increases this agreement becomes progressively worse. As seen in Sec. V, mutual excitations and two-phonon excitations, which are not included in CCMOD, become progressively more significant with increasing Z_1Z_2, particularly when there is a state with very large β_λ, as in ^{28}Si. An extended version of CCMOD, known as CCMPH [30], allows double-phonon and mutual excitations to be included and very much better agreement with experimental data can be achieved using this code. A calculation for $^{35}Cl+^{92}Zr$, using the same double- and mutual-phonon couplings as described in Sec.V D, is shown in Fig. 5 to illustrate this point. However such simplified programs might not be expected to give accurate results due to the approximate treatment of the excitation energies of the excited states and to the use of the linear coupling approximation. In the cases reported here, the projectiles have high excitation energies and deformations β, hence realistic CC calculations are desirable. To treat the coupling correctly, the CC code CCFULL was used and the results are discussed in the next section.

V. REALISTIC COUPLED-CHANNELS CALCULATIONS

The CC code CCFULL [15] has been used in an attempt to obtain satisfactory fits to each of the four systems measured,

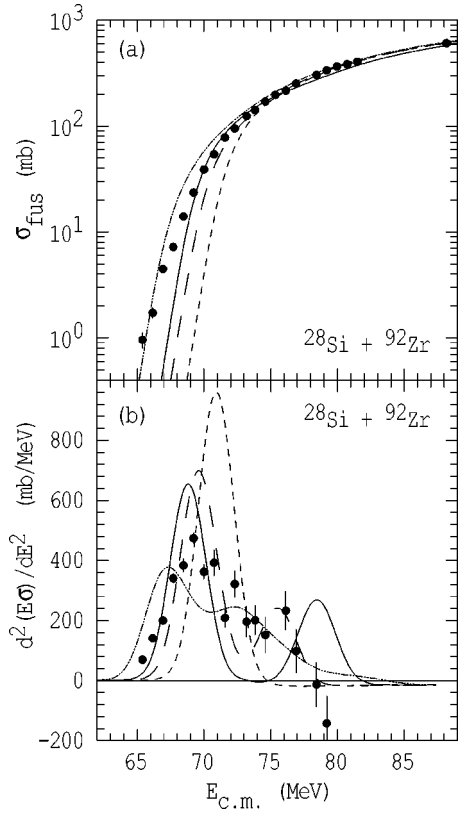

FIG. 4. The experimental (a) fusion cross sections and (b) barrier distribution for ^{28}Si + ^{92}Zr, the latter evaluated with $\Delta E_{\text{c.m.}} = 2.30$ MeV. The lines represent CCMOD calculations for the single barrier (dashed lines), with coupling including only states in ^{92}Zr (long dashed lines), and, in addition, the 1.78 MeV state of ^{28}Si taken as a phonon state (solid lines) and an oblate rotational state (dot-dot-dashed lines).

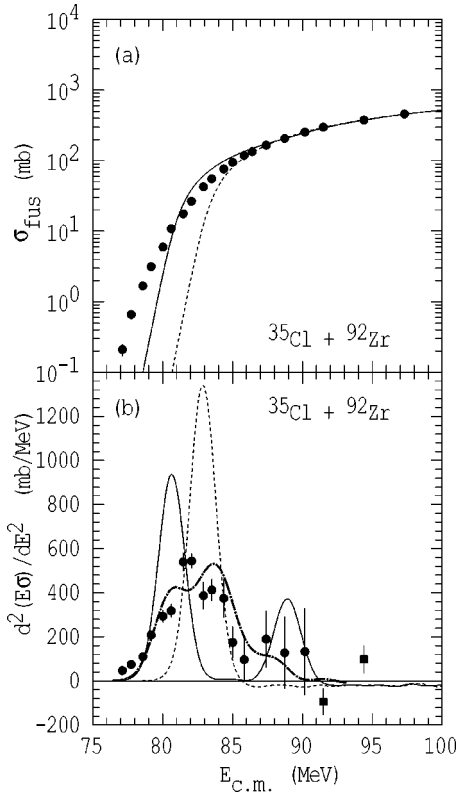

FIG. 5. The experimental (a) fusion cross sections and (b) barrier distribution for ^{35}Cl+^{92}Zr, the latter evaluated with $\Delta E_{\text{c.m.}} = 1.45$ MeV. The two points represented by the squares were calculated with $\Delta E_{\text{c.m.}} = 2.90$ MeV. The dashed and solid lines result from CCMOD calculations for a single barrier and for both ^{92}Zr states plus four states in ^{35}Cl, respectively. The thick dot-dashed line shows the barrier distribution resulting from a calculation with the extended simplified CC code CCMPH, which included single- and double-quadrupole- and octupole-phonon states in ^{92}Zr and all mutual couplings between states in the target and projectile.

using a consistent set of parameters. This code treats couplings to all orders, and takes proper account of finite excitation energies and Coulomb excitation. It uses the ingoing-wave boundary condition inside the Coulomb barrier to account for fusion, along with the isocentrifugal approximation, which works well for heavy ions [31,32]. The version of CCFULL used allowed for the inclusion of two excited states in the target nucleus and one in the projectile, with the option of including multiphonon or multirotational states based on them, and mutual excitations between all of them.

Unfortunately it was not possible to include transfer reactions in the analyses because CCFULL does not treat coupling to these channels correctly. The low-energy cross sections, well below the average barrier are especially sensitive to transfer reactions with positive Q values. Such reactions exist for the ^{28}Si and ^{35}Cl induced reactions, with Q values for the two-neutron pickup equal to $+3.25$ and $+3.06$ MeV, respectively, but not for the lighter systems.

There are a number of uncertainties involved in CC analyses of inelastic scattering and fusion. A few are mentioned here but much more detail is given, for example, by Satchler [21]. In order to obtain physically meaningful descriptions of the measured fusion data, values for β_λ are required. Usually these are derived from experimental values of $B(E\lambda)\uparrow$, resulting from measurements of Coulomb excitation, γ-ray lifetimes, or electron scattering, with the relationship given in Eq. (4). This relationship is a first order result, applying to a transition from the ground state 0^+ to λ, obtained by integrating over the nuclear charge distribution whose density depends on $(r-R)$, which is often taken to have the WS form. For large values of β_λ, as occur in light nuclei such as ^{28}Si, significant deviations from this result can occur [33] and the series expansion does not quickly converge. There is also a weak dependence on the diffuseness parameter a. In

TABLE III. Parameters for the real nuclear potential determined by fitting the high-energy fusion cross sections with r_0 fixed at 0.80 fm. Also shown is the average fusion barrier B_0.

Reaction	V_0 (MeV)	r_0 (fm)	a (fm)	B_0 (MeV)
^{12}C+^{92}Zr	358.2	0.80	0.91	32.3
^{16}O+^{92}Zr	702.5	0.80	0.85	42.0
^{28}Si+^{92}Zr	468.6	0.80	1.03	70.9
^{35}Cl+^{92}Zr	261.7	0.80	1.35	82.9

these calculations we have used the first order result but the limited validity of the relationship given in Eq. (4) for light nuclei should be kept in mind.

When measurements by electromagnetic methods are not available, the β_λ, or more usually the deformation length $\delta=\beta_\lambda R$, are often taken from deformed optical-model analyses of nuclear scattering data. There are a number of possible problems with such results. There is an uncertainty in the definition of the nuclear potential, which is usually taken to have the WS form for convenience, though there is no real justification for this. The deformation parameter for the optical-model potential is not in general the same as that for the density distribution, even for nucleon scattering, and even less so for the scattering of composite nuclei. Nuclear scattering involves the complex interactions between nucleons, with the nuclear *n-n* and *p-p* forces differing from the n-p force. However electromagnetic measurement of $B(E\lambda)\uparrow$ relates only to the density distribution of the protons and the simple long-range Coulomb interaction. Thus the deformation parameters for nuclear, β_λ^N, and Coulomb β_λ^C, interactions may differ and also be dependent on shell effects [34] in the projectile and target nuclei. Indeed such differences have been reported. For example, Takagui *et al.* [35] found good fits to the data with $\beta_2^N=0.25$ as compared with $\beta_2^C=0.108$ for the first 2^+ state of ^{92}Zr. This value was obtained from a coupled-channels analysis of the scattering of ^{16}O by ^{92}Zr using $r_c=1.2$ fm in Eq. (4), though various uncertainties prevent this result from being definitive. The ratio β_2^N/β_2^C was much smaller with the lighter α, proton, and neutron projectiles. No such large difference was reported for the first 3^- state.

The value one should take for r_c is not entirely clear. In the earlier coupled-channels analyses of Refs. [12,36], a value of $r_c=1.06$ fm, with $\beta_\lambda^N=\beta_\lambda^C$ was often used. In this paper, following Ref. [35], r_c has been chosen to be 1.2 fm. The correct value to choose for this quantity is not presently known but is likely to lie somewhere between 1.06 and 1.2 fm. If say a value of 1.2 fm is chosen for r_c and $\beta_2^N/\beta_2^C>1$, then an approximately similar result from a coupled-channels calculation can be achieved with a smaller value of r_c and $\beta_\lambda^N=\beta_\lambda^C$. This can be seen from the inelastic coupling term to first order,

$$F_{\rm inel}(r)=\frac{\beta_\lambda}{\sqrt{4\pi}}\left[-R^{(p)}\frac{dV_n(r)}{dr}+\frac{3Z_1Z_2e^2}{(2\lambda+1)}\frac{R^{(p)\lambda}}{r^{\lambda+1}}\right], \quad (5)$$

where $R^{(p)}$ is the equivalent sharp-surface radius of the nucleus excited, which together with Eq. (4) yields

$$F_{\rm inel}(r)=\frac{\sqrt{4\pi}}{3Z}\left[\frac{B(E\lambda)\uparrow}{e^2}\right]^{1/2}\left[-(R^{(p)})^{1-\lambda}\frac{dV_n(r)}{dr}+\frac{3Z_1Z_2e^2}{(2\lambda+1)}\frac{1}{r^{\lambda+1}}\right]. \quad (6)$$

Hence, for a given value of $B(E\lambda)\uparrow$, the nuclear part of this coupling term is proportional to $(R^{(p)})^{1-\lambda}$, while the Coulomb part is independent of $R^{(p)}$, as it should be. Thus decreasing the value of r_c is equivalent to increasing the value of β_λ^N [see Eq. (4)]. However it should be appreciated that the value of $\beta_\lambda^N/\beta_\lambda^C$ is not necessarily the same for every state or for the same state excited by different projectiles [21,35].

The choice of parameters for the real WS potential used in the more exact coupled-channels codes such as CCFULL requires consideration. For correct operation, the code CCFULL requires rather deeper potentials than would be achieved with a radius parameter of $r_0\approx 1.20$ fm. In the barrier region the nuclear potential varies approximately exponentially with *r*. Therefore it is possible to achieve deeper potentials with smaller values of r_0 while retaining essentially the same values for the nuclear potential in the barrier region. In these calculations, values for $r_0=0.80$ fm were used.

In contrast to the behavior of the CCMOD calculations, the effect of inclusion of excited states with finite excitation energies ϵ_x in CCFULL is to reduce the average fusion barrier energy compared with that for the one-dimensional barrier which fits the high-energy cross sections. This can be understood as a polarization effect. In the adiabatic situation, when the period of the nuclear vibration is much shorter than the tunneling time, that is $\epsilon_x \gg \hbar\omega_0$ (the curvature of the average barrier), the system has sufficient time to respond to the nuclear force in such a way that the barrier is reduced [18,37,38]. This effect occurs to a lesser extent even when $\epsilon_x \leqslant \hbar\omega$. Further, the inclusion of higher-order couplings increases the widths of the potential barriers, and hence decreases $\hbar\omega$ over the uncoupled value [18]. Therefore, since the average barrier shifts according to the couplings employed in CCFULL calculations, the potential parameters have to be adjusted to fit the high-energy cross sections after the couplings are altered. The single-barrier prescription already implicitly includes the effects of coupling to all states in the target and projectile, as well as transfer couplings. In view of the considerable time taken to make individual coupled-channels calculations, it was decided to attempt only reasonably good fits to the high-energy cross sections, which were consequently slightly worse than those using the best fit parameters.

Following Ref. [35], a radius parameter of $r_c=1.2$ fm was used in the CCFULL calculations that follow. To investigate the difference between β_2^N and β_2^C for ^{92}Zr, found in the analysis of the inelastic scattering of ^{16}O from ^{92}Zr [35], the value of β_2^N was varied from $\beta_2^N=\beta_2^C$ in order to optimize the fit to the data. For ^{92}Zr, values of $\beta_2^C=0.103$ and $\beta_3^C=0.17$ were used in all calculations. The latter result derives from proton inelastic-scattering measurements [29], and has a large uncertainty of ± 0.03. For the octupole-phonon state β_3^N was taken to be equal to β_3^C. The CCFULL calculations include coupling up to two-phonon excitations [39] for the 2_1^+ and 3_1^- states in ^{92}Zr, and one-phonon or one-roton excitation in the projectile nucleus. All possible mutual excitations of the projectile and target nuclei are included. The coupling scheme employed in the CCFULL calculations, and the quality of fit to the data, is discussed for each reaction below.

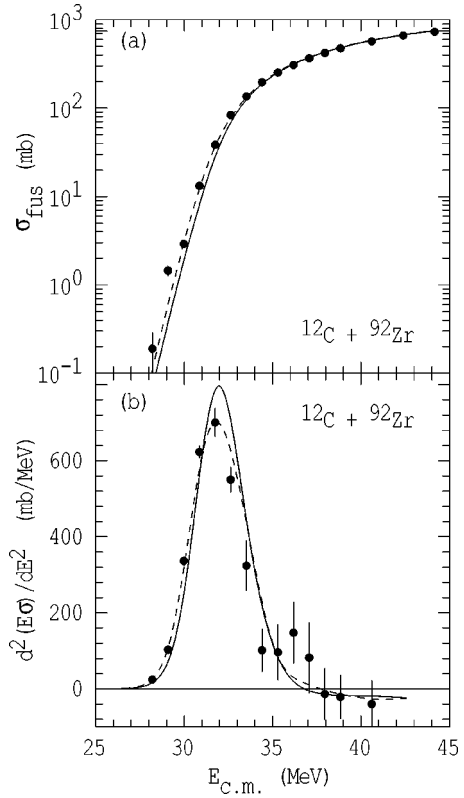

FIG. 6. Comparison of the measured (a) fusion cross sections and (b) barrier distribution for $^{12}C+^{92}Zr$ with CC calculations using the code CCFULL. The results shown are for two-phonon excitations in ^{92}Zr with $\beta_2^N=0.144$ (solid line) and $\beta_2^N=0.20$ (dashed line). Single-phonon calculations give results which differ insignificantly from these.

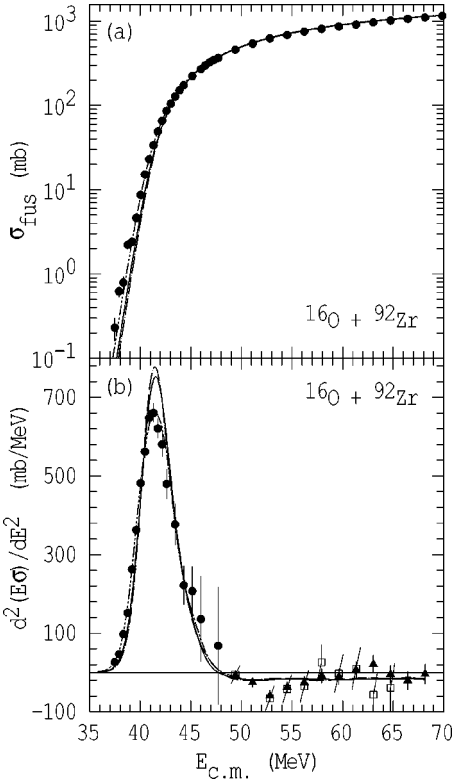

FIG. 7. Comparison of the measured (a) fusion cross sections and (b) barrier distribution for $^{16}O+^{92}Zr$ with CCFULL calculations. Shown are results for two-phonon coupling with $\beta_2^N=0.144$ (solid line) and $\beta_2^N=0.20$ (dash-dot-dotted line). Also shown is the coupling to the single phonon for the $\beta_2^N=0.144$ case only (dashed-dotted line).

A. The $^{12}C+^{92}Zr$ reaction

The results from the CCFULL calculation for the $^{12}C+^{92}Zr$ reaction are shown in Fig. 6. The β_2 value of the 4.44 MeV 2^+ state in ^{12}C was taken to be -0.592. A good reproduction of the measured barrier distribution was obtained with two different values for the target deformation parameter, $\beta_2^N=0.144$ and 0.20, the latter being somewhat better. As might be expected for this system, there is an almost negligible difference in the shape of the fusion barrier distribution between the one-phonon and two-phonon coupling schemes. It was also found that the treatment of the 2_1^+ state in ^{12}C had little effect on the results, whether it is taken to be a phonon or rotational state.

B. The $^{16}O+^{92}Zr$ reaction

For the $^{16}O+^{92}Zr$ reaction, shown in Fig. 7, the difference between the $\beta_2^N=0.144$ and $\beta_2^N=0.20$ calculations is similar to that obtained for the $^{12}C+^{92}Zr$ reaction, with $\beta_2^N=0.20$ giving a much better fit to the barrier peak. A small difference between the single- and two-phonon couplings for $\beta_2^N=0.144$ is seen. Calculations for $^{16}O+^{92}Zr$ in Refs. [40,41] suggested that coupling to both the single- and two-phonon excitations in ^{92}Zr might produce significant barrier strength at energies well above the barrier centered at $E_{c.m.}\simeq 42$ MeV. For this reason measurements were made at much higher energies above the average barrier than for the other reactions. Two separate measurements were performed, with the first measurement (squares in Fig. 7) suggesting that there might be such strength in the region of $E_{c.m.}\simeq 60$ MeV. A subsequent measurement with better statistics (solid triangles in Fig. 7) showed that such an effect, if present, is very weak.

It should be noted that $d^2(E_{c.m.}\sigma_{fus})/dE_{c.m.}^2$ is expected to become slightly negative, and to remain so, at energies above the average barrier. This is because the mean fusion radius decreases with increasing angular momentum and hence increasing energy. Thus the return of the barrier distribution to positive or even zero values over a significant energy range might indicate the presence of a higher barrier. In contrast to the CC calculations of Refs. [40,41], the CCFULL calculations in Fig. 7, which include the 3^- state in ^{16}O with $\beta_3=0.57$ [29], give little if any indication of the presence of higher barriers. However the calculations differ in that, in the earlier work [40,41], not all mutual couplings nor the 3^- state in ^{16}O were included and the large value of $\beta_2^N=0.25$ from Ref. [35] was used. Thus the existence of higher barriers with significant weight seems to be ruled out by both experiment and the CCFULL calculations.

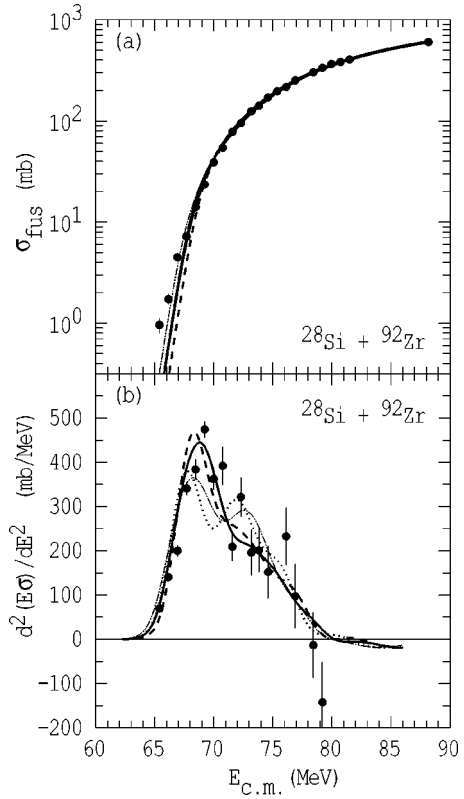

FIG. 8. Comparison of measured (a) fusion cross sections and (b) barrier distribution for ^{28}Si + ^{92}Zr with CCFULL calculations. Results are shown for both single- and two-phonon coupling in ^{92}Zr with $\beta_2^N = 0.144$ and the first excited state in ^{28}Si taken as a phonon state (thick dashed and full lines, respectively) and taken as an oblate rotor (dotted and dash-dot-dotted lines, respectively).

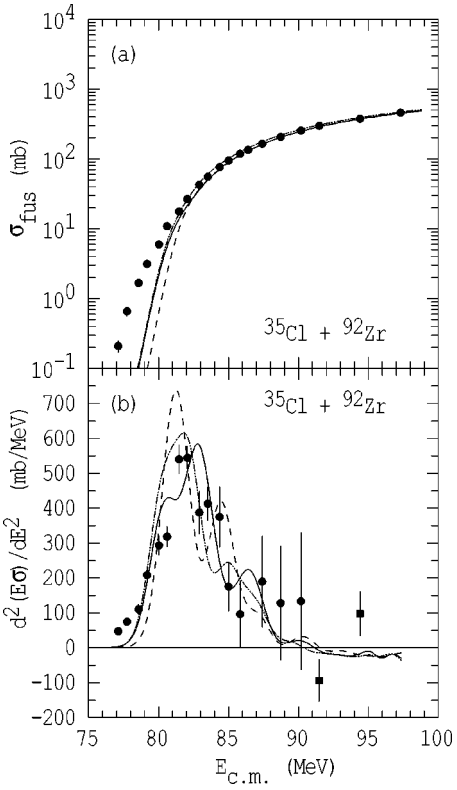

FIG. 9. Comparison of measured (a) fusion cross sections and (b) barrier distribution for ^{35}Cl+^{92}Zr with CCFULL calculations. Results are shown for single- (dashed lines) and two-phonon coupling (solid lines) in ^{92}Zr with $\beta_2^N = 0.144$ and $r_c = 1.2$ fm and for two-phonon coupling with $\beta_2^N = \beta_2^C$ and $r_c = 1.06$ fm (dash-dot-dot line). The first four states in ^{35}Cl were included (see text).

C. The ^{28}Si+^{92}Zr reaction

The results of the CCFULL calculations for the ^{28}Si+^{92}Zr reaction are shown in Fig. 8. All calculations were made with $\beta_2^N = 0.144$. In Fig. 8, a comparison, for single-phonon coupling in ^{92}Zr, is made between taking the 2^+ state in ^{28}Si as a phonon state (thick dashed line) or as an oblate [42,43] rotor (dotted line), with $\beta_2 = -0.407$ for ^{28}Si. Also compared are the two-phonon coupling in ^{92}Zr and the single-phonon state in ^{28}Si (thick solid line) and the oblate case (dash-dot-dotted lines). From these calculations it can be seen that treating the 2^+ state in ^{28}Si as a phonon state rather than as an oblate rotor gives a somewhat better fit, while calculations with two-phonon coupling give somewhat better fits than with single-phonon coupling.

Treating the 2^+ state in ^{28}Si as a prolate rotor, or taking $\beta_2^N = 0.20$ for ^{92}Zr (neither shown), give poor representations of the data. It seems likely that varying the parameters a little would allow good fits to the data for all of the cases shown in Fig. 8 and hence there is not strong evidence to distinguish between the presence of single- and two-phonon excitations in ^{92}Zr or between ^{28}Si being vibrational or oblate. The fits to the lower-energy cross sections would probably be improved with inclusion of the positive Q value transfer reactions, such as the two-neutron pickup channel at $Q = +3.25$ MeV.

D. The ^{35}Cl+^{92}Zr reaction

The CC calculations for the ^{35}Cl induced reaction are shown in Fig. 9. There are a number of states in ^{35}Cl which might contribute to the channel coupling. Since the code CCFULL only allows coupling to one type of vibrational mode in the projectile, the β_2 of the states at 1.219, 1.763, 2.646, and 2.694 MeV in ^{35}Cl were combined in quadrature and the energy taken as 1.763 MeV. In this case, including two-phonon excitations in ^{92}Zr gives a noticeably better fit than with one, as shown by the solid and dashed lines in Fig. 9, respectively. For comparison, a calculation with $r_c = 1.06$ fm and $\beta_2^N = \beta_2^C$ for ^{92}Zr is also shown (dash-dot-dotted lines in Fig. 9) and this gives a fit of similar quality. Again, inclusion of transfer channels would probably improve the fit to the lower-energy cross sections and fusion barrier distribution. For example, the two-neutron pickup channel has $Q = +3.06$ MeV.

Some calculations were performed with a WS-squared form of the nuclear potential for the above reactions. These gave similar results to CCFULL calculations with the WS form of the nuclear potential.

VI. DISCUSSION

The coupled-channels calculations described above indicate that it is possible to reproduce the barrier distributions

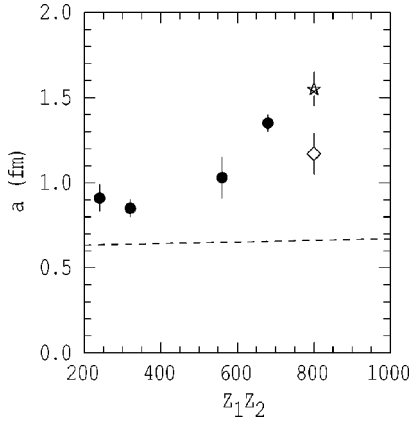

FIG. 10. The diffuseness parameter *a*, determined from fits to the high-energy cross sections with $r_0=0.8$ fm, as a function of Z_1Z_2 for a selection of reactions involving Zr nuclei. The solid circles relate to the measurements with ^{92}Zr, the open diamond to ^{40}Ca+^{90}Zr [39], and the open star to ^{40}Ca+^{96}Zr (Ref. [39]). The dashed line is an empirical relationship (Ref. [45] derived from elastic-scattering data).

and high-energy cross sections quite well with a radius parameter of 1.2 fm in Eq. (4) and with the same set of deformation parameters for ^{92}Zr. From this analysis, it seemed necessary to have $\beta_2^N > \beta_2^C$, a value of $\beta_2^N=0.144$ being a reasonable compromise for all four projectiles. A better fit could be obtained for ^{12}C and ^{16}O with a larger value for $\beta_2^N=0.20$, which however gave a worse fit for the two heavier projectiles. A value of $\beta_2^N=0.25$, as used in Ref. [35], is too large for all cases considered here. However, as discussed in Sec.V, β_2^N need not be the same for different reactions. The inclusion of two-phonon states in the coupling scheme seemed to improve the reproduction of the shape of the measured barrier distribution, particularly for the heavier projectiles.

Although the present representations of the data are not perfect, further calculations were not performed because of the current restrictions on the number of states which can be included in the CCFULL calculations, the lack of a correct treatment of transfer, and other uncertainties such as the lack of direct knowledge of two-phonon states and their degree of anharmonicity [36,44]. There also remains the problem that the diffuseness parameters obtained from fusion analyses are much larger than those from elastic-scattering measurements. A summary of the diffuseness parameters obtained from the fits to the high-energy data in this work is shown in Fig. 10. The error bars indicate the ranges which increase the minimum χ^2 values by 1. These values of *a* were obtained with $r_0=0.8$ fm (see Sec. III), but only slightly smaller values for *a* resulted when a larger value for the radius parameter, for example $r_0=1.00$ fm, was used. Values for the reactions ^{40}Ca+^{90}Zr and ^{96}Zr [39] are also included in Fig. 10. For these six reactions, the fitted values for *a* generally increase with increasing Z_1Z_2. This behavior is compared with values obtained from the empirical relationship given by Broglia and Winther [45] in their Eq. III.1.44. However the above should not necessarily be taken as a general result as, for example, the system ^{28}Si+^{144}Sm requires a value for *a* of

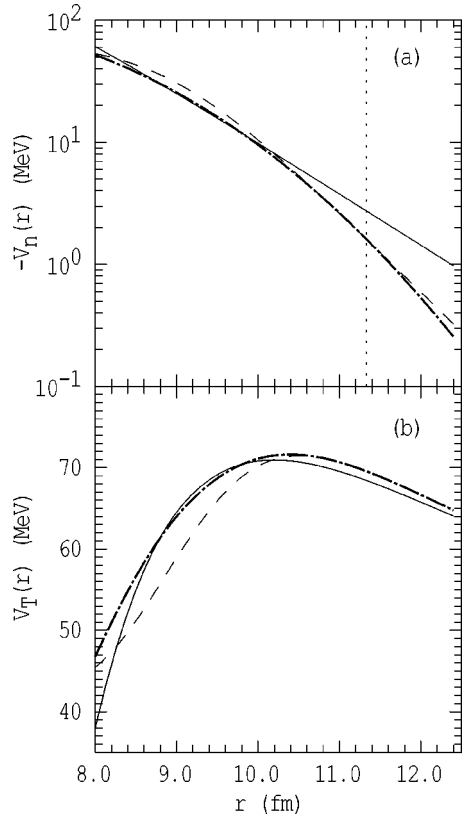

FIG. 11. Nuclear potentials are shown in (a) for the case ^{28}Si +^{92}Zr. That derived from fitting the high-energy fusion data measured in this work (full line) is compared with the empirical potential of Ref. [45] which fits elastic-scattering data (dashed line) and the potential with a Gaussian type falloff (thick dot-dashed line), which is forced to fit the dashed line at the strong-coupling radius R_{sc} (vertical dotted line). The corresponding total potentials V_T for zero angular momentum, the sums of the nuclear and Coulomb potentials, are shown in (b). Values for B_0 for the three potentials are 70.94, 71.46, and 71.62 MeV and for $\hbar\omega_0$ 3.35, 3.97, and 3.44 MeV, respectively.

only 0.90 ± 0.15, even though $Z_1Z_2=868$. Further, the large difference between the values for ^{40}Ca+^{90}Zr and ^{96}Zr suggests that nuclear structure effects may be contributing.

It has been shown [21,46,47] that, for a given form of nuclear potential, good fits to elastic scattering data result from potentials which intersect in a narrowly defined region of the separation distance *r*. The value of *r* where this intersection occurs corresponds roughly to the strong-coupling radius R_{sc}, which has a value of approximately $1.5(A_1^{1/3}+A_2^{1/3})$ fm. Even when the potentials do not have the same form this criterion still applies, though less strongly [46].

Nuclear potentials as a function of *r* are shown in Fig. 11(a) for the ^{28}Si+^{92}Zr reaction. The corresponding total potentials $V_T(r)=V_n(r)+V_{\rm Coul}(r)$ are shown in Fig. 11(b). The dashed lines relate to the empirical WS potential of Ref. [45], which is expected to fit elastic scattering well, and the full lines are derived from fitting the high-energy fusion data in this work [see Eq. (3) and Table III]. These two potentials, which are of the same form, do not come close to intersecting near the strong-coupling radius, $R_{sc}=11.3$ fm in this

case. This implies that the potential that fits the high-energy fusion data will not be able to fit the elastic scattering. If this anomaly is primarily due to the form of potential, it appears from Fig. 11(a) that a potential which falls more rapidly with increasing r than the WS form is required. Powers of WS up to 3 do not fall rapidly enough. A potential with a Gaussian type falloff with r may be able to match the elastic-scattering potential at R_{sc}. A potential was chosen to be of the form

$$V_n(r) = -V_0 \frac{erfc(x)}{2}, \tag{7}$$

where $x=(r-r_0A_P^{1/3}-r_0A_T^{1/3})/a$. Such a potential, shown by the thick dot-dashed line in Fig. 11(a), was forced to intersect with the dashed line at R_{sc}. This potential would probably fit the elastic-scattering data reasonably well. It gives an almost identical value for $\hbar\omega_0$ to that from the potential that fits the high-energy fusion data and a slightly higher value for B_0, as can be seen in Fig. 11(b). Cross sections for the high-energy fusion depend mainly on B_0 and $\hbar\omega_0$ [4]. Calculations with a modified version of CCFULL, for the uncoupled case with the Gaussian potential, reproduce the experimental data fairly well, in spite of the fact that no attempt was made to optimize the parameters. Optimization would almost certainly produce an excellent fit but is pointless at the present stage in view of the arbitrary shape chosen for the potential and the uncertainty in the value of the crossing radius.

It therefore appears likely that one could choose a potential form that could fit both fusion and elastic-scattering data. However, whether a more rapidly falling potential could be the full or partial explanation of the anomaly remains an open question. More work is required, both experimentally on obtaining further systematics on the diffuseness parameter for fusion, and theoretically on calculating the elastic and fusion channels (simultaneously) with a complete CC model and a less arbitrary choice of nuclear potential.

VII. CONCLUSIONS

The fusion cross sections for the reactions ^{12}C, ^{16}O, ^{28}Si, and ^{35}Cl on ^{92}Zr have been measured to high precision and barrier distributions obtained. Satisfactory reproductions of these barrier distribution shapes have been obtained using the ''exact'' coupled-channels code CCFULL. With a expression for the coupling radius of the excited nucleus given by $r_c=1.2A^{1/3}$ fm, better fits were achieved with $\beta_2^N>\beta_2^C$ for the first excited state of ^{92}Zr, though not to the extent of that found in Ref. [35]. Perfect fits were neither obtained nor attempted due to limitations of the CC code regarding the number of excited states which can be included and the non-inclusion of transfer reactions, probably important for the ^{28}Si and ^{35}Cl induced reactions.

The diffuseness parameters of the real nuclear potentials for each measured reaction were again found to be larger than those expected from analyses of elastic scattering data. The results for the four reactions measured in this work, together with those for ^{40}Ca+^{90}Zr and ^{96}Zr [39], suggest an increase in a as the charge product Z_1Z_2 of the reaction increases. However, drawing general conclusions from this limited data set might be dangerous. There is also an indication that nuclear structure effects may play a part. Elastic scattering probes larger separation distances of the two nuclei than does fusion. It is suggested that a nuclear potential, which falls off more rapidly with r than the WS potential, might explain, at least in part, the anomalous behavior of a. This merits further investigation.

ACKNOWLEDGMENTS

We would like to thank Dr. N. Rowley for discussions regarding the ^{16}O+^{92}Zr reaction. We are grateful for the support of Dr. D. C. Weisser and the technical staff of the 14UD Pelletron accelerator.

[1] C. Y. Wong, Phys. Lett. **42B**, 186 (1972).
[2] L. C. Vaz and J. M. Alexander, Phys. Rev. C **10**, 464 (1974); **18**, 2152 (1978).
[3] R. G. Stokstad, Y. Eisen, S. Kaplanis, D. Pelte, U. Smilansky, and I. Tserruya, Phys. Rev. C **21**, 2427 (1980).
[4] M. Dasgupta, D. J. Hinde, N. Rowley, and A. M. Stefanini, Annu. Rev. Nucl. Part. Sci. **48**, 401 (1998), and references therein.
[5] C. H. Dasso, S. Landowne, and A. Winther, Nucl. Phys. **A405**, 381 (1983); **A407**, 221 (1983).
[6] R. A. Broglia, C. H. Dasso, S. Landowne, and A. Winther, Phys. Rev. C **27**, 2433 (1983); R. A. Broglia, C. H. Dasso, S. Landowne, and G. Pollarolo, Phys. Lett. **133B**, 34 (1983).
[7] N. Rowley, G. R. Satchler, and P. H. Stelson, Phys. Lett. B **254**, 25 (1991).
[8] J. X. Wei, J. R. Leigh, D. J. Hinde, J. O. Newton, R. C. Lemmon, S. Elfström, J. X. Chen, and N. Rowley, Phys. Rev. Lett. **67**, 3368 (1991).
[9] R. C. Lemmon, J. R. Leigh, J. X. Wei, C. R. Morton, D. J. Hinde, J. O. Newton, J. C. Mein, M. Dasgupta, and N. Rowley, Phys. Lett. B **316**, 32 (1993).
[10] J. R. Leigh, N. Rowley, R. C. Lemmon, D. J. Hinde, J. O. Newton, J. X. Wei, J. C. Mein, C. R. Morton, S. Kuyucak, and A. T. Kruppa, Phys. Rev. C **47**, R437 (1993).
[11] C. R. Morton, M. Dasgupta, D. J. Hinde, J. R. Leigh, R. C. Lemmon, J. P. Lestone, J. C. Mein, J. O. Newton, H. Timmers, N. Rowley, and A. T. Kruppa, Phys. Rev. Lett. **72**, 4074 (1994).
[12] J. R. Leigh, M. Dasgupta, D. J. Hinde, J. C. Mein, C. R. Morton, R. C. Lemmon, J. P. Lestone, J. O. Newton, H. Timmers, J. X. Wei, and N. Rowley, Phys. Rev. C **52**, 3151 (1995).
[13] C. H. Dasso and S. Landowne, Comput. Phys. Commun. **46**, 187 (1987); J. Fernández-Niello, C. H. Dasso, and S. Landowne, *ibid.* **54**, 409 (1989).
[14] M. Dasgupta, A. Navin, Y. K. Agerwal, C. V. K. Baba, H. C. Jain, M. L. Jhingan, and A. Roy, Nucl. Phys. **A539**, 351 (1992).
[15] K. Hagino, N. Rowley, and A. T. Kruppa, Comput. Phys. Commun. **123**, 143 (1999).

[16] H. Esbensen and S. Landowne, Phys. Rev. C **35**, 2090 (1987).
[17] H. Esbensen and B. B. Back, Phys. Rev. C **54**, 3109 (1996).
[18] K. Hagino, N. Takigawa, M. Dasgupta, D. J. Hinde, and J. R. Leigh, Phys. Rev. C **55**, 276 (1997).
[19] D. M. Brink, *Semi-Classical Methods For Nucleus-Nucleus Scattering* (Cambridge University Press, Cambridge, 1985).
[20] J. Błocki, J. Randrup, W. J. Świątecki, and C. F. Tsang, Ann. Phys. (N.Y.) **105**, 427 (1977).
[21] G. R. Satchler, *Direct Nuclear Reactions* (Oxford University Press, New York, 1983), Chap. 14.
[22] J. X. Wei, J. R. Leigh, D. C. Weisser, J. O. Newton, S. Elfström, J. P. Lestone, J. X. Chen, D. G. Popescu, and D. J. Hinde, Nucl. Instrum. Methods Phys. Res. A **306**, 557 (1991).
[23] P. P. Tung, K. A. Erb, M. W. Sachs, G. B. Sherwood, R. J. Ascuitto, and D. A. Bromley, Phys. Rev. C **18**, 1663 (1978).
[24] A. Gavron, Phys. Rev. C **21**, 230 (1980).
[25] M. Dasgupta, D. J. Hinde, J. R. Leigh, R. C. Lemmon, J. C. Mein, C. R. Morton, J. O. Newton, and H. Timmers, in *Proceedings of the the International Workshop on Heavy-Ion Fusion*, edited by A. M. Stefanini *et al.* (World Scientific, Singapore, 1994), p. 115.
[26] C. Y. Wong, Phys. Rev. Lett. **31**, 766 (1973).
[27] N. Rowley, J. R. Leigh, J. X. Wei, and R. Lindsay, Phys. Lett. B **314**, 179 (1993).
[28] S. Raman, C. H. Malarkey, W. T. Milner, C. W. Nestor, Jr., and P. H. Stelson, At. Data Nucl. Data Tables **36**, 1 (1986).
[29] R. H. Spear, At. Data Nucl. Data Tables **42**, 55 (1989).
[30] M. Dasgupta, Australian National University Department of Nuclear Physics Report ANU-P1333, 1997 (unpublished).
[31] K. Hagino, N. Takigawa, A. B. Balantekin, and J. R. Bennett, Phys. Rev. C **52**, 286 (1995), and references therein.
[32] M. A. Nagarajan, N. Rowley, and R. T. Lindsay, J. Phys. G **12**, 529 (1986).
[33] A. Bohr and B. R. Mottelson, *Nuclear Structure*, (Benjamin, New York, 1975), Vol. II, p. 139.
[34] V. A. Madsen, V. R. Brown, and J. D. Anderson, Phys. Rev. C **12**, 1205 (1975).
[35] E. M. Takagui, G. R. Satchler, H. Takai, K. Koide, and O. Dietzsh, Nucl. Phys. **A514**, 120 (1990).
[36] C. R. Morton, A. C. Berriman, M. Dasgupta, D. J. Hinde, J. O. Newton, K. Hagino, and I. J. Thompson, Phys. Rev. C **56**, 2104 (1997).
[37] K. Hagino, N. Takigawa, and A. B. Balantekin, Phys. Rev. C **56**, 2104 (1997).
[38] K. Hagino, N. Takigawa, M. Dasgupta, D. J. Hinde, and J. R. Leigh, J. Phys. G **23**, 1413 (1997).
[39] H. Timmers, D. Ackermann, S. Beghini, L. Corradi, J. H. He, G. Montagnoli, F. Scarlassara, A. M. Stefanini, and N. Rowley, Nucl. Phys. **A663**, 421 (1998).
[40] N. Rowley, Nucl. Phys. **A538**, 205c (1992).
[41] A. T. Kruppa, P. Romain, M. A. Nagarajan, and N. Rowley, Nucl. Phys. **A560**, 845 (1993).
[42] P. Möller, J. R. Nix, W. D. Myers, and W. J. Świątecki, At. Data Nucl. Data Tables **59**, 185 (1995).
[43] P. Raghavan, At. Data Nucl. Data Tables **42**, 189 (1989).
[44] K. Hagino, N. Takigawa, and S. Kuyucak, Phys. Rev. Lett. **79**, 2943 (1997).
[45] R. A. Broglia and A. Winther, *Heavy Ion Reactions Lecture Notes, Volume I: Elastic and Inelastic Reactions* (Benjamin/Cummings, Reading, 1981).
[46] M. H. Macfarlane and S. C. Pieper, Phys. Lett. **103B**, 169 (1981).
[47] M. Lozano and G. Madurga, Nucl. Phys. **A334**, 349 (1990).